Inorganic Chemistry

Article

pubs.acs.org/IC

9-Oxidophenalenone: A Noninnocent β-Diketonate Ligand?

Amit Das,[†] Thomas Michael Scherer,[‡] Shaikh M. Mobin,[†] Wolfgang Kaim,*[,‡] and Goutam Kumar Lahiri*[,†]

[†]Department of Chemistry, Indian Institute of Technology Bombay, Powai, Mumbai 400076, India

[‡]Institut für Anorganische Chemie, Universität Stuttgart, Pfaffenwaldring 55, D-70550 Stuttgart, Germany

Supporting Information

ABSTRACT: The redox systems $[Ru(L)(bpy)_2]^k$, $[Ru(L)_2(bpy)]^m$, and $[Ru(L)_3]^n$ containing the potentially redox-active ligand 9-oxidophenalenone = L^- were investigated by spectroelectrochemistry (UV−vis−near-IR and electron paramagnetic resonance) in conjunction with density functional theory (DFT) calculations. Compounds $[Ru(L^-)(bpy)_2]ClO_4$ ($[\mathbf{1}]ClO_4$) and $[Ru(L^-)_2(bpy)]ClO_4$ ($[\mathbf{2}]ClO_4$) were structurally characterized. In addition to establishing electron-transfer processes involving the $Ru^{II}/Ru^{III}/Ru^{IV}$ and $bpy^0/bpy^{\bullet-}$ couples, evidence for the noninnocent behavior of L^- was obtained from $[Ru^{IV}(L^{\bullet})(L^-)(bpy)]^{3+}$, which exhibits strong near-IR absorption due to ligand-to-ligand charge transfer. In contrast, the lability of the electrogenerated anion $[Ru(L)_2(bpy)]^-$ is attributed to a resonance situation $[Ru^{II}(L^{\bullet 2-})(L^-)(bpy)]^-/[Ru^{II}(L^-)_2(bpy^{\bullet-})]^-$, as suggested by DFT calculations.

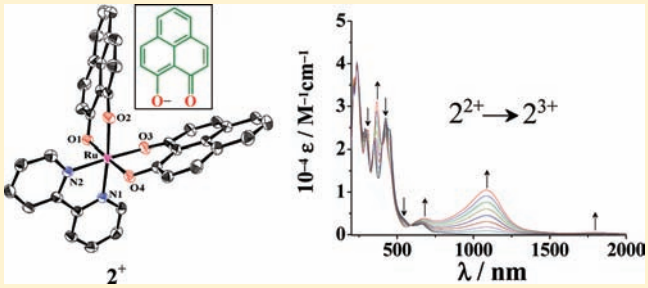

INTRODUCTION

The β-diketonates are among the most frequently used ligands in applied coordination chemistry, forming stable chelates with all metal ions and permitting volatility, e.g., for metal−organic chemical vapor deposition (MOCVD) and related techniques.[1,2] Despite their unsaturated character with π-electron delocalization, the most common β-diketonates, especially 2,4-pentanedionate (acetylacetonate, $acac^-$) and its alkylated and/or fluorinated derivatives, have usually not been considered as redox-active "noninnocent" ligands. However, a recent report on a nickel complex of NacNac, i.e., involving an O/NR-exchanged β-diketiminate, has been analyzed as exhibiting "hidden noninnocence", viz., containing an oxidized ligand on the basis of magnetic measurements.[3]

Our own uses of the $acac^-$ ligand, in combination with ruthenium coordination chemistry,[4] have suggested a potential of β-diketonates for partial intramolecular electron transfer with suitable metal centers, based on density functional theory (DFT) calculations aimed at understanding experimental properties such as spin distribution. To enhance and probe such tendencies, we have now chosen to investigate ruthenium complexes of 9-oxidophenalenone, L^- (**X**).

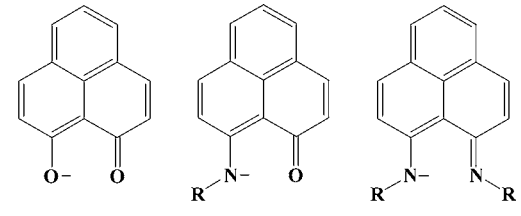

L^- = **X** **Y** **Z**

The underlying phenalenyl π system of **X**−**Z** is known to undergo electron transfer, and the 1,9-substituted chelate ligands (**Y** and **Z**) have been studied in complexes with the positively charged Lewis acid centers B^{III}, Al^{III}, Si^{IV}, and Ge^{IV}.[5] Electrochemical *reduction* of these species was interpreted as involving ligand-based stepwise electron uptake;[5c] the equally plausible oxidation of the anionic ligand has not yet been discussed.

Invoking ruthenium as the central metal with its intricate coordination behavior toward noninnocent ligands,[4] we now present the first complexes of the 9-oxidophenalenone ligand with a redox-active transition metal and describe the synthesis, characterization, and theoretical analysis of the redox systems $[Ru(L)(bpy)_2]^k$, $[Ru(L)_2(bpy)]^m$, and $[Ru(L)_3]^n$.

RESULTS AND DISCUSSION

Synthesis and Characterization. The diamagnetic complex $[Ru^{II}(L)(bpy)_2]ClO_4$ ($[\mathbf{1}]ClO_4$) and the paramagnetic complexes $[Ru^{III}(L)_2(bpy)]ClO_4$ ($[\mathbf{2}]ClO_4$) and $Ru^{III}(L)_3$ (**3**) (L^- = 9-oxidophenalenone; bpy = 2,2′-bipyridine) have been synthesized from the precursors $Ru^{II}(bpy)_2Cl_2·2H_2O$, $Ru^{III}(bpy)Cl_3·H_2O$, and $RuCl_3·3H_2O$, respectively, in the presence of 9-hydroxy-1*H*-phenalen-1-one and the base NEt_3 under a dinitrogen atmosphere (see the Experimental Section). The presence of two or three electron-donating ligands L^- in the complex framework of $[\mathbf{2}]ClO_4$ and **3** stabilizes the metal ion in the Ru^{III} state.

Received: January 28, 2012
Published: March 21, 2012

 © 2012 American Chemical Society dx.doi.org/10.1021/ic300207d | *Inorg. Chem.* 2012, 51, 4390−4397

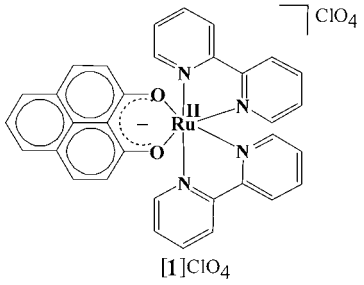

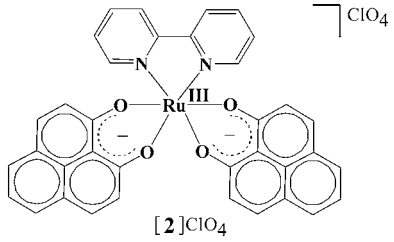

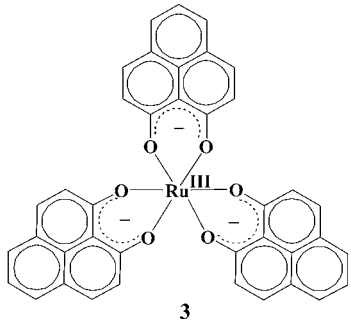

3

The identities of the complexes have been established by their satisfactory microanalytical, conductivity and electrospray ionization mass spectrometry (ESI-MS; Figure S1 in the Supporting Information, SI) data. The ^{1}H NMR spectrum of the diamagnetic [**1**]ClO_4 in $(CD_3)_2SO$ exhibits partial overlap of the 23 proton signals within the chemical shift range of 6−10 ppm. The ^{1}H NMR spectra of [**2**]ClO_4 in $(CD_3)_2SO$ and of **3** in $CDCl_3$ show proton resonances in the wide chemical shift ranges of −10 to +25 and −4 to +13 ppm, respectively, due to paramagnetic contact shifts (Figure S2 in the SI and the Experimental Section).[6] Accordingly, the isolated ruthenium(III) complexes [**2**]ClO_4 and **3** exhibit electron paramagnetic resonance (EPR) spectra typical for metal-based spin (Figure 4 and Table 6).

Structural Aspects. The identities of the complexes [**1**]ClO_4 and [**2**]ClO_4 have been authenticated by single-crystal X-ray structures (Figures 1 and 2). Selected crystallographic and bond parameters are given in Tables 1−3. In [**1**]ClO_4 or [**2**]ClO_4, the ligand (L^-) binds to the central Ru atom through the O-donor atoms, forming a six-membered chelate ring. The trans and cis angles around the Ru ion deviate slightly from the idealized 180° and 90°, respectively, implying a distorted octahedral situation. The average Ru−N(bpy) distance trans to the O(L) donor in [**1**]ClO_4 is ∼0.02 Å shorter than that trans to the N(bpy) donor, reflecting the trans effect of the σ-donating O center and the π-acceptor character of the bpy ligand. The average Ru^{II}−O(L) and Ru^{III}−O(L) distances of 2.035 and 1.994 Å in [**1**]ClO_4 and [**2**]ClO_4, respectively, match fairly well with analogous structures containing {Ru^{II}-acac} and {Ru^{III}-acac} fragments (acac$^-$ = 2,4-pentanedionato).[4a,d,7] Similarly, the average Ru^{II}−N(bpy) and Ru^{III}−N(bpy) distances of 2.021 and 2.034 Å in [**1**]ClO_4 and [**2**]ClO_4, respectively, are in agreement with those reported for standard {Ru-bpy} complexes.[8] The bond parameters involving coordinated L are similar to those reported for the structurally characterized germanium(IV), silicon(IV), aluminum(III) complexes of L.[5b,c] The Ru atoms in [**1**]ClO_4 and [**2**]ClO_4 deviate from the plane of L by 5.92° and 14.3°/15.15°, respectively. Similar deviations (∼12°) have been reported for germanium(IV) and silicon(IV) complexes of L.[5b] The average

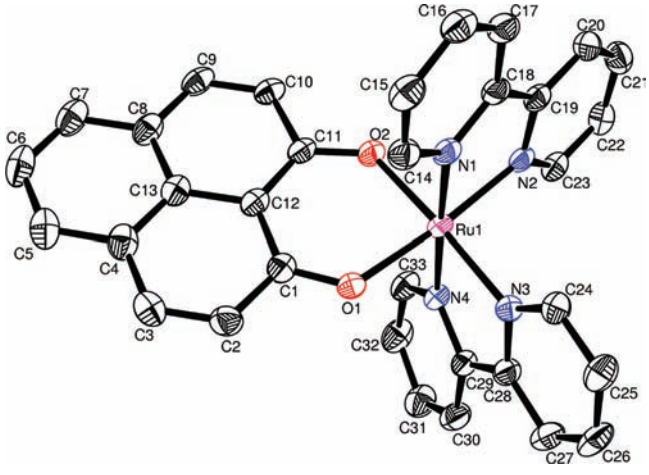

Figure 1. ORTEP diagram of the cationic part of [**1**]ClO_4. Ellipsoids are drawn at the 50% probability level. H atoms, the perchlorate anion, and the solvent of crystallization are omitted for clarity.

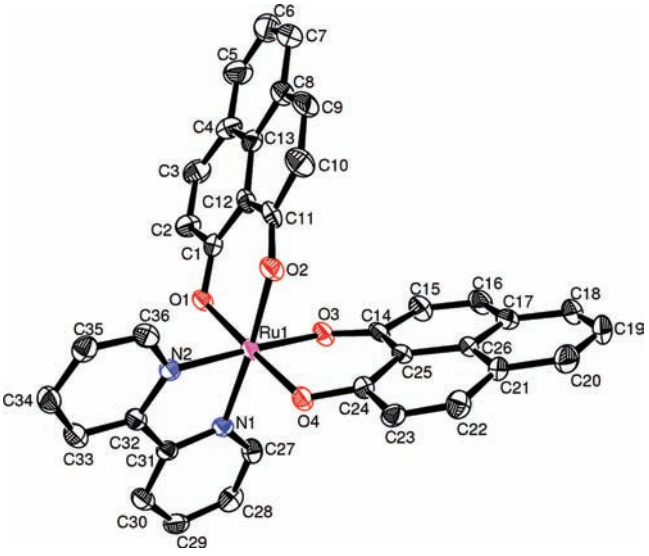

Figure 2. ORTEP diagram of the cationic part of [**2**]ClO_4. Ellipsoids are drawn at the 50% probability level. H atoms, the perchlorate anion, and the solvent of crystallization are omitted for clarity.

dx.doi.org/10.1021/ic300207d | Inorg. Chem. 2012, 51, 4390−4397

Table 1. Selected Crystallographic Data for $[1]ClO_4$ and $[2]ClO_4$

	$[1]ClO_4 \cdot 2C_6H_6$	$[2]ClO_4 \cdot C_7H_8$
empirical formula	$C_{39}H_{29}ClN_4O_6Ru$	$C_{43}H_{30}ClN_2O_8Ru$
fw	786.18	839.21
cryst syst	triclinic	monoclinic
space group	$P\bar{1}$	$P2_1/n$
a (Å)	11.7451(4)	7.3674(8)
b (Å)	12.5229(4)	6.3139(3)
c (Å)	13.5292(4)	32.319(2)
α (deg)	111.013(3)	90
β (deg)	97.520(2)	97.976(5)
γ (deg)	112.200(3)	90
V (Å^3)	1636.17(9)	3509.7(3)
Z	2	4
μ (mm^{-1})	0.618	0.585
T (K)	120(2)	150(2)
D_{calcd} (g cm^{-3})	1.596	1.588
$F(000)$	800	1708
θ range (deg)	3.35–25.00	3.29–25.00
data/restraints/param	5732/0/460	6184/0/497
R1, wR2 [$I > 2\sigma(I)$]	0.0336, 0.0900	0.0396, 0.0906
R1, wR2 (all data)	0.0371, 0.0916	0.0617, 0.0953
GOF	1.052	0.967
largest diff peak/hole (e Å^{-3})	0.859/−1.026	0.847/−0.396

Table 2. Selected Bond Distances (Å) and Bond Angles (deg) for $[1]ClO_4 \cdot 2C_6H_6$

bond distance (Å)		bond angle (deg)	
Ru1–N2	2.0210(19)	N2–Ru1–N3	95.54(8)
Ru1–N3	2.022(2)	N2–Ru1–O1	173.30(7)
Ru1–O1	2.0337(16)	N3–Ru1–O1	87.80(7)
Ru1–N1	2.035(2)	N2–Ru1–N1	79.14(8)
Ru1–O2	2.0373(16)	N3–Ru1–N1	98.29(8)
Ru1–N4	2.041(2)	O1–Ru1–N1	94.66(7)
O1–C1	1.285(3)	N2–Ru1–O2	86.39(7)
O2–C11	1.289(3)	N3–Ru1–O2	174.76(7)
C1–C12	1.437(3)	O1–Ru1–O2	90.79(7)
C1–C2	1.452(3)	N1–Ru1–O2	86.86(7)
C2–C3	1.351(4)	N2–Ru1–N4	101.07(8)
C3–C4	1.424(4)	N3–Ru1–N4	79.28(8)
C4–C5	1.404(4)	O1–Ru1–N4	85.24(7)
C4–C13	1.421(4)	N1–Ru1–N4	177.57(7)
C5–C6	1.381(4)	O2–Ru1–N4	95.57(7)
C6–C7	1.385(4)		
C7–C8	1.401(4)		
C8–C13	1.419(4)		
C8–C9	1.427(4)		
C9–C10	1.354(4)		
C10–C11	1.437(3)		
C11–C12	1.442(3)		
C12–C13	1.443(3)		

C–O(L) bond distances in $[1]ClO_4$ and $[2]ClO_4$ of 1.287 and 1.288 Å, respectively, imply a delocalized situation, as is generally observed in metal β-diketonate complexes [average C–O(acac) distances: $Ru(acac)_3$, 1.282 Å; $Co(acac)_2$, 1.270 Å; $Cu(acac)_2$, 1.273 Å].[9,10]

The bond angles and bond distances of DFT (B3LYP/LANL2DZ/6-31G*)-optimized $\mathbf{1}^+$ and $\mathbf{2}^+$ (Figure S3a,b in the SI) are in agreement with the experimentally obtained values (Tables 2 and 3 and S1 and S2 in the SI).

Table 3. Selected Bond Distances (Å) and Bond Angles (deg) for $[2]ClO_4 \cdot C_7H_8$

bond distance (Å)		bond angle (deg)	
Ru1–O4	1.976(2)	O4–Ru1–O3	90.69(9)
Ru1–O3	1.994(2)	O4–Ru1–O1	178.28(10)
Ru1–O1	1.996(2)	O3–Ru1–O1	88.23(9)
Ru1–O2	2.010(2)	O4–Ru1–O2	88.78(10)
Ru1–N2	2.031(3)	O3–Ru1–O2	88.16(10)
Ru1–N1	2.036(3)	O1–Ru1–O2	89.85(10)
O1–C1	1.284(4)	O4–Ru1–N2	90.94(10)
O2–C11	1.279(4)	O3–Ru1–N2	175.21(11)
O3–C14	1.286(4)	O1–Ru1–N2	90.25(10)
O4–C24	1.303(4)	O2–Ru1–N2	96.38(10)
		O4–Ru1–N1	92.44(10)
		O3–Ru1–N1	96.58(11)
		O1–Ru1–N1	89.01(10)
		O2–Ru1–N1	175.08(10)
		N2–Ru1–N1	78.85(11)

In spite of several attempts, we failed to grow suitable single crystals of complex **3**. The DFT-optimized structure of **3** (Figure S3c and Table S3 in the SI) was calculated with an average Ru–O bond distance of 2.089 Å, longer than the average experimental Ru^{III}–O distance of 2.003 Å in $Ru(acac)_3$.[9]

The Redox Series. On the basis of electrochemical transformations as studied by cyclic voltammetry (CV) and differential pulse voltammetry (Figure 3 and Table 4), the spectroelectrochemical results [EPR and UV–vis–near-IR (NIR); Figures 4 and 6–8 and Tables 5 and 6] were obtained and discussed in conjunction with DFT calculation data (Figure 5 and Tables 7 and S4–S23 in the SI).

Redox Series $[Ru(L)(bpy)_2]^k$. The structurally characterized diamagnetic complex cation (k = +1) from the isolated $[Ru(L)(bpy)_2]ClO_4$ contains ruthenium(II), stabilized through two π-accepting bpy coligands. A metal-to-ligand charge-transfer (MLCT) absorption band at 520 nm, involving transitions to π^*(bpy) and $\pi^*(L^-)$, is observed (Figure 6) and confirmed by time-dependent (TD-DFT) calculations (Table S13 in the SI). Stepwise reduction occurs for the two bpy ligands at negative potentials with characteristically separated waves (Figure 3a and Table 4), causing the diminishing and then disappearance of the bpy-targeted MLCT absorption (Figure 6b,c) and the emergence of very weak intraligand transitions in the NIR region and more intense absorption around 550 nm (Tables 5 and S14 and S15 in the SI), typical for $bpy^{\bullet-}$ and its complexes.[11,12] The one-electron reduction to the neutral intermediate $[Ru^{II}(L^-)(bpy^{\bullet-})(bpy)]^0$ = **1** produces a single-line EPR signal at 2.006 (Figure 4), as established for several other ruthenium(II) complexes of reduced α-diimines;[13] the calculated spin densities (Figure 5 and Table 7) confirm this result.

Oxidation of the cation to the dication leads to $[Ru^{III}(L^-)(bpy)_2]^{2+}$ = $\mathbf{1}^{2+}$, as is evident from the EPR signal with its large g anisotropy (Figure 4 and Table 6) due to the high spin–orbit coupling constant of the spin-bearing $4d^5$-configured Ru ion.[14] The calculated spin densities (Figure 5 and Table 7) confirm the predominantly metal-centered unpaired electron in $\mathbf{1}^{2+}$. Accordingly, the MLCT band at 520 nm is replaced by a weaker ligand-to-metal charge-transfer (LMCT) absorption $\pi(L^-) \rightarrow d\pi(Ru^{III})$ at 780 nm (Figure 6a and Tables 5 and S16 in the SI). The second oxidation step proved to be irreversible,

dx.doi.org/10.1021/ic300207d | Inorg. Chem. 2012, 51, 4390–4397

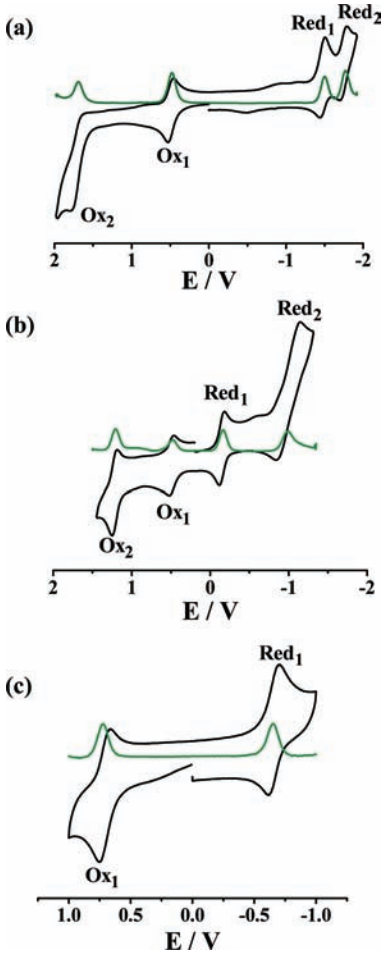

Figure 3. Cyclic voltammograms (black lines) and differential pulse voltammograms (green lines) of (a) $[\mathbf{1}]ClO_4$, (b) $[\mathbf{2}]ClO_4$, and (c) **3** in acetonitrile/0.1 M NEt_4ClO_4 at 298 K. Scan rate: 100 mV s^{-1}. The second oxidation wave in part a and the second reduction wave in part b are distorted in CV because of the proximity to the solvent limit.

Table 4. Electrochemical Data[a] for $[\mathbf{1}]ClO_4$, $[\mathbf{2}]ClO_4$, and 3

	$E_{298}°$/V (ΔE_p/mV)[b]			
complex	Ox_2	Ox_1	Red_1	Red_2
$\mathbf{1}^+$	1.78 (ir)	0.50(70)	−1.48(70)	−1.74(80)
$\mathbf{2}^+$	1.23(70)	0.49(60)	−0.15(70)	−0.99(300)
3		0.71(90)	−0.66(90)	

[a]From CV in CH_3CN/0.1 M Et_4NClO_4 at 100 mV s^{-1}. [b]Potential in V versus SCE; peak potential differences ΔE_p [mV] (in parentheses).

which suggests contributions from the $Ru^{III}(L^{\bullet})$ alternative in addition to the $Ru^{IV}(L^-)$ form (Scheme 1); the oxidative formation of more labile neutral ligands is known to enhance dissociation, as is known from the electrochemistry of complexes with quinone-type ligands.

Redox Series [Ru(L)$_3$]^n. The isolated neutral form (n = 0) is formulated as a ruthenium(III) species, based on the EPR signal (Figure 4 and Table 6) . The EPR data correspond to those (2.9 > g > 1.2) reported for $Ru(acac)_3$[15] albeit with shifted g-component values (Table 6). This reflects the lower-lying occupied β-diketonate orbitals in the case of the acac system, while the destabilized molecular orbitals (MOs) of L^- not only lead to facilitated oxidation but also to a closer highest occupied molecular orbital (HOMO)−single occupied molecular orbital (SOMO) distance and thus to increase g values.[16] The calculated spin densities (Figure 5 and Table 7) confirm the metal-centered spin.

As proven coulometrically, the complex $[Ru(L)_3]$ = **3** exhibits only one reversible one-electron reduction and one one-electron oxidation within the accessible potential range of ±2.0 V versus SCE (Figure 3 and Table 4). Upon one-electron reduction to an EPR-silent anion (n = −1) involving ruthenium(II), the homoleptic tris-chelate complex shows the

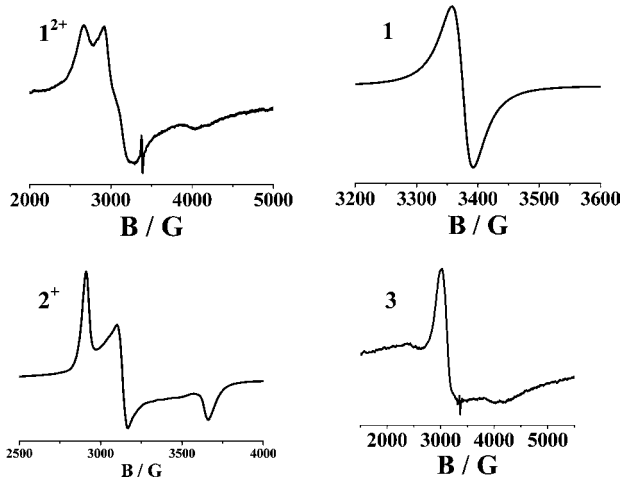

Figure 4. EPR spectra of $\mathbf{1}^{2+}$, **1**, $\mathbf{2}^+$ and **3** in acetonitrile/0.1 M Bu_4NPF_6 at 110 K.

Table 5. UV−vis−NIR Spectroelectrochemical Data for $\mathbf{1}^n$ (n = 2+, +, 0), $\mathbf{2}^n$ (n = 3+, 2+, +, 0), and $\mathbf{3}^n$ (n = +, 0, −) in CH_3CN/0.1 M Bu_4NPF_6

compound	λ [nm] (ε [M^{-1} cm^{-1}])
$\mathbf{1}^{2+}$	780 (2950), 500 (sh, 3000), 425 (28600), 400 (sh, 19200), 300 (29800), 240 (37050)
$\mathbf{1}^+$	520 (21700), 390 (14450), 370 (14950), 345 (17900), 295 (47250), 240 (33450)
1	520 (17650), 385 (11850), 370 (12400), 345 (14650), 295 (43550), 240 (28650)
$\mathbf{1}^-$	1510 (390), 585 (sh, 12950), 440 (21300), 380 (sh, 14600), 295 (38400), 240 (31600)
$\mathbf{2}^{3+}$	1090 (10450), 670 (3800), 425 (23350), 370 (31100), 300 (24550), 240 (38950)
$\mathbf{2}^{2+}$	800 (450), 650 (2500), 450 (sh, 24500), 425 (27200), 350 (21950), 290 (24700), 235 (40550)
$\mathbf{2}^+$	655 (sh, 2650), 530 (sh, 7950), 450 (25050), 425 (23850), 350 (21950), 290 (29200), 240 (39000)
2	640 (19100), 590 (sh, 17800), 400 (17600), 385 (sh, 16400), 345 (sh, 16200), 300 (43000), 230 (43100)
$\mathbf{3}^+$	780 (6800), 450 (21800), 425 (sh, 18500), 365 (31400), 310 (sh, 11500), 235 (39000)
3	590 (sh, 3900), 490 (24200), 420 (sh, 11800), 350 (21900), 260 (sh, 25100), 235 (31400)
$\mathbf{3}^-$	1000 (sh, 4941), 790 (24300), 490 (sh, 2000), 390 (sh, 11050), 325 (30200), 240 (37900)

Table 6. EPR Parameters from Measurements at 110 K in CH_3CN/0.1 M Bu_4NPF_6

compound	g_1	g_2	g_3	g_{iso}	$\Delta g = g_1 - g_3$
1	[a]	[a]	[a]	2.0060	<0.01
$\mathbf{1}^{2+}$	2.539	2.204[b]	1.68	2.141	0.860
$\mathbf{2}^+$	2.323	2.156	1.846	2.108	0.477
3	3.00	2.142	1.64	2.26	1.36

[a]Not resolved. [b]Shoulder.

dx.doi.org/10.1021/ic300207d | Inorg. Chem. 2012, 51, 4390−4397

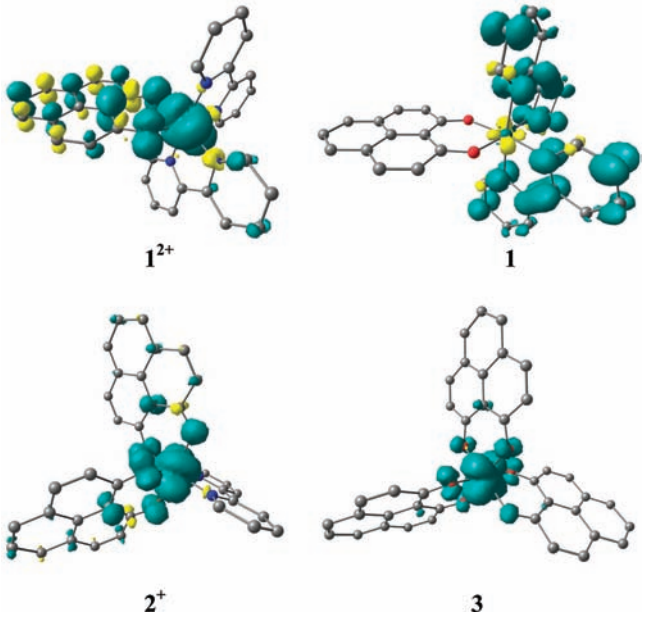

Figure 5. DFT calculated spin density plots of 1^{2+}, **1**, 2^{+} and **3**.

Table 7. DFT-Calculated Mulliken Spin Densities for Paramagnetic Complexes

	Ru	L	bpy
$[Ru(L)(bpy)]^0$	−0.034	−0.001	1.036
$[Ru(L)(bpy)_2]^{2+}$	0.703	0.253	0.050
$[Ru(L)_2(bpy)]^+$	0.749	0.246	0.005
$[Ru(L)_3]$	0.806	0.193	

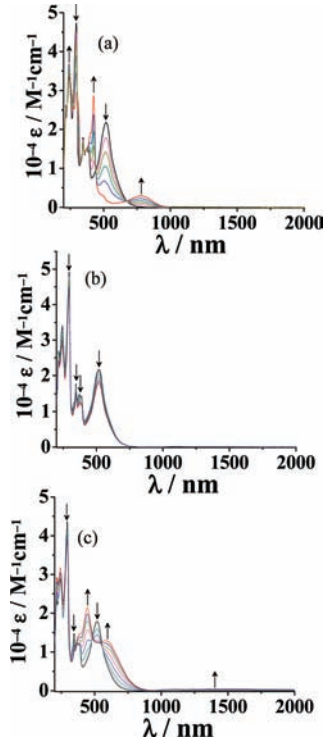

Figure 6. UV−vis−NIR spectroelectrochemistry for the conversions of (a) $1^+ \rightarrow 1^{2+}$, (b) $1^+ \rightarrow 1$, and (c) $1 \rightarrow 1^-$ in CH_3CN/0.1 M Bu_4NPF_6.

Scheme 1

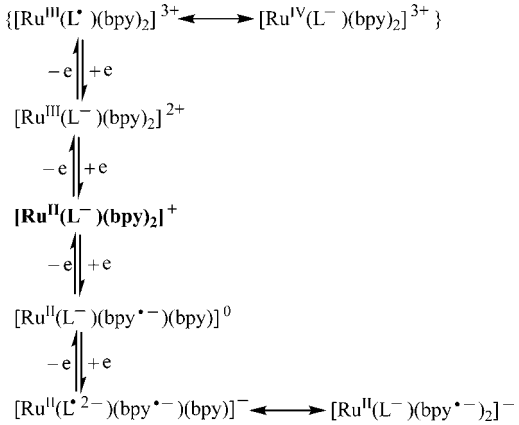

disappearance of the LMCT absorption at 490 nm (Table S17 in the SI) and the emergence of a long-wavelength band system above 700 nm (Figure 7), which is attributed to MLCT transitions involving the relatively low-lying[5c] π^* MO of L^-.

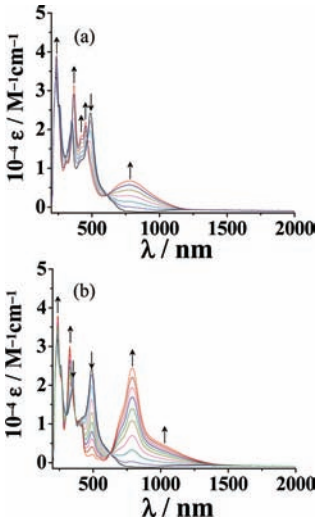

Figure 7. UV−vis−NIR spectroelectrochemistry for the conversions of (a) $3 \rightarrow 3^+$ and (b) $3 \rightarrow 3^-$ in CH_3CN/0.1 M Bu_4NPF_6.

TD-DFT calculations support this assignment of the main absorption at 790 nm (Table S18 in the SI); the low-energy shoulder is tentatively attributed to a triplet transition becoming allowed because of the high spin−orbit coupling constant of ruthenium.[14] The oxidation to $[Ru(L)_3]^+ = 3^+$ can lead to $Ru^{III}(L^{\bullet})$ or $Ru^{IV}(L^-)$ alternative (Scheme 2). In the absence of EPR information and considering the DFT results (Tables S10 and S11 in the SI), we postulate appreciable contributions from both of these resonance forms; in any case,

Scheme 2

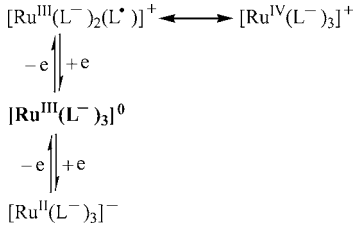

dx.doi.org/10.1021/ic300207d | Inorg. Chem. 2012, 51, 4390−4397

the observed low-energy absorption at 780 nm can be assigned to a LMCT transition (see the TD-DFT results; Table S19 in the SI).

Redox Series [Ru(L)$_2$(bpy)]^m. According to crystal structure analysis, revealing short Ru−O bonds, and to the EPR spectrum (Figure 4), in conjunction with the results from spin-density calculations (Figure 5 and Table 7), the cation **2**$^+$ in the isolated complex [Ru(L$^-$)$_2$(bpy)]ClO$_4$ contains ruthenium(III), despite the presence of one π-accepting bpy ligand. However, the compound is rather easily reduced and oxidized (Figure 3 and Table 4); the comproportionation constant for [Ru(L)$_2$(bpy)]$^+$ is only $K_c = 10^{10.8}$. The first reduction produces the expected EPR-silent neutral ruthenium(II) complex **2** (Scheme 3), which shows the LMCT absorption features around 450 nm for the cation (Table S20 in the SI) being replaced by MLCT absorption bands involving transitions to π^*(bpy) and π^*(L$^-$) target orbitals at longer wavelengths at about 600 nm (Figure 8 and Tables 5 and S21 in the SI). The second reduction wave at −0.99 V does not exhibit reversible electron transfer. We attribute this lability to contributions from both L$^-$/bpy$^{\bullet-}$ and L$^{\bullet 2-}$/bpy^0 formulations, i.e., a mixed L$^-$- and bpy-based reduction, in agreement with the previously reported reducibility of coordinated ligands such as L$^-$.[5c]

Scheme 3

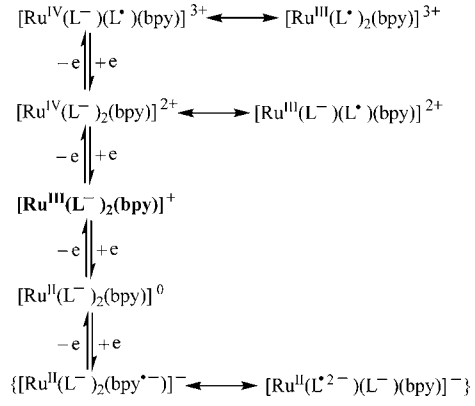

One-electron oxidation of [Ru^{III}(L$^-$)$_2$(bpy)]$^+$ leads to an EPR-silent dication **2**$^{2+}$ with few changed absorption features (Figure 8 and Table 5), in agreement with a Ru^{III} → Ru^{IV} transition. The alternative Ru^{III}/L$^\bullet$ formulation (Scheme 3) appears less plausible and is not supported by the TD-DFT calculation results (Table S22 in the SI).

A significant spectral change is observed for the second oxidation to [Ru(L)$_2$(bpy)]$^{3+}$ (Figure 8b and Tables 5 and S23 in the SI). An intense NIR absorption emerges at 1090 nm during the reversible process, which we take as a clear indication for ligand-based electron removal. Ligand-to-ligand intervalence charge transfer (LLIVCT) transitions are well-known. e.g., from catecholate/semiquinone/quinone coordination chemistry;[17] they tend to produce broad absorption bands at low energies. We therefore assume a description of [Ru^{IV}(L$^\bullet$)(L$^-$)(bpy)]$^{3+}$ as most appropriate for the trication, with minor contribution from the alternative [Ru^{III}(L$^\bullet$)$_2$(bpy)]$^{3+}$ formulation (Scheme 3). TD-DFT calculations reproduce the NIR absorption and confirm ligand-based transitions as the major components (Table S23 in the SI). An EPR signal for the electrogenerated trication was not observed, possibly because of low-lying excited states facilitating rapid EPR relaxation.

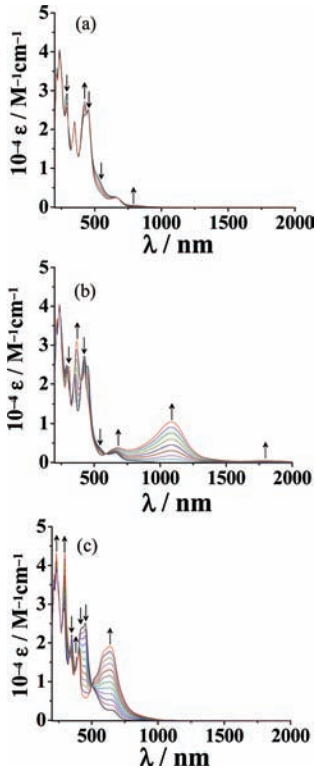

Figure 8. UV−vis−NIR spectroelectrochemistry for the conversions of (a) **2**$^+$ → **2**$^{2+}$, (b) **2**$^{2+}$ → **2**$^{3+}$, and (c) **2**$^+$ → **2** in CH$_3$CN/0.1 M Bu$_4$NPF$_6$.

The formulation [Ru^{IV}(L$^\bullet$)(L$^-$)(bpy)]$^{3+}$ for the electrogenerated trication reflects the potential for oxidation of electron-rich β-diketonates, here enhanced through the presence of the delocalized phenalenyl π system. The formulation [Ru^{IV}(L$^\bullet$)(L$^-$)(bpy)]$^{3+}$ and the long-wavelength absorption are also related to the form [Fe^{IV}(Por$^{\bullet-}$)(O)(X)]$^{2+}$ of highly oxidized heme intermediates in P450 monooxygenases and peroxidases, where an Fe^{IV} center is coupled to a porphyrinato(−) radical ligand (Por$^{\bullet-}$) following oxidation.[18]

CONCLUDING REMARKS

The aim of this study has been to probe the potential for noninnocent ligand behavior of an apparently redox-active β-diketonate, 9-oxidophenalenone (L$^-$). Calculated spin densities (Figures S4 and S5 in the SI) and electronic transitions (Figures S6 and S7 and Tables S24 and S25 in the SI) reveal O,O′-localized spin for L$^\bullet$ (as noted earlier[19]) and no significant absorption in the visible region, while the reduced form L$^{\bullet 2-}$accepts electron density in the phenalenyl π system,[20] showing absorptivity around 390 and 434 nm (Figure S7 in the SI).

The investigations revealed only one instance, **2**$^{3+}$, when a ligand-based oxidation was evident from spectroscopy, as confirmed by TD-DFT calculations. In several other cases within the series [Ru(L)(bpy)$_2$]^k, [Ru(L)$_2$(bpy)]^m, and [Ru(L)$_3$]^n, oxidation of the metal or reduction of the bpy coligands were established by spectroelectrochemistry. The formation of the previously invoked[5c] reduced state, L$^{\bullet 2-}$, could not be observed in the present situation because of electrochemical irreversibility. In conclusion, however, not only NacNac

dx.doi.org/10.1021/ic300207d | Inorg. Chem. 2012, 51, 4390−4397

derivatives but also modified β-diketonates can thus act as noninnocent ligands albeit in a hidden way.[3,21]

EXPERIMENTAL SECTION

Materials. The starting metal complexes $Ru(bpy)Cl_3·H_2O$[22] and the ligand 9-hydroxy-1*H*-phenalen-1-one[23] (HL) were prepared according to the reported procedures. $RuCl_3·3H_2O$ was purchased from Aldrich. Other chemicals and solvents were of reagent grade and were used as received. For spectroscopic and electrochemical studies, HPLC-grade solvents were used.

Instrumentation. UV−vis−NIR studies were performed in CH_3CN/0.1 M Bu_4NPF_6 at 298 K using an optically transparent thin layer electrode cell mounted in the sample compartments of a J&M Tidas spectrophotometer.[24] ^1H NMR spectra were recorded on a Bruker Avance III 400 spectrometer. The EPR measurements were made in a two-electrode capillary tube with an X-band Bruker ESP300 system, equipped with a Bruker ER035 M gaussmeter and a HP 5350B microwave counter. Cyclic voltammetric, differential pulse voltammetric, and coulometric measurements were performed using a PAR model 273A electrochemistry system with platinum wire working and auxiliary electrodes and an aqueous saturated calomel reference electrode (SCE) in a three-electrode configuration. The supporting electrolyte was Et_4NClO_4, and the solute concentration was $\sim 10^{-3}$ M. The half-wave potential $E_{298}{}^{\circ}$ was set equal to $0.5(E_{pa} + E_{pc})$, where E_{pa} and E_{pc} are anodic and cathodic cyclic voltammetric peak potentials, respectively. Elemental analysis was carried out with a Perkin-Elmer 240C elemental analyzer. ESI MS spectra were recorded on a Micromass Q-ToF mass spectrometer.

Crystallography. Single crystals of $[\mathbf{1}]ClO_4$ and $[\mathbf{2}]ClO_4$ were grown by the slow evaporation of a 1:1 acetonitrile/benzene solution of $[\mathbf{1}]ClO_4$ and a 1:2 dichloromethane/toluene solution of $[\mathbf{2}]ClO_4$. The crystal data were collected on an Oxford X-CALIBUR-S CCD diffractometer. Selected data collection parameters and other crystallographic results are summarized in Table 1. All data were corrected for Lorentz polarization and absorption effects. The program package of *SHELX-97*[25] was used for structure solution and full-matrix least-squares refinement on F^2. H atoms were included in the refinement using the riding model.

Computational Details. Full geometry optimizations were carried out using the DFT method at the (R)B3LYP level for $\mathbf{1}^{3+}$, $\mathbf{1}^{+}$, $\mathbf{2}^{2+}$, **2**, $\mathbf{3}^{+}$, and $\mathbf{3}^{-}$ and the (U)B3LYP level for $\mathbf{1}^{2+}$, **1**, $\mathbf{2}^{3+}$, $\mathbf{2}^{+}$, $\mathbf{2}^{-}$, and **3**.[26] All elements except Ru were assigned the 6-31G(d) basis set. The LANL2DZ basis set with an effective core potential was employed for the Ru atom.[27] Vibrational frequency calculations were performed to ensure that the optimized geometries represent the local minima and there are only positive eigenvalues. All calculations were performed with the *Gaussian03* program package.[28] Vertical electronic excitations based on (U)B3LYP/(R)B3LYP-optimized geometries were computed for **1**, $\mathbf{1}^{+}$, $\mathbf{1}^{2+}$, **2**, $\mathbf{2}^{+}$, $\mathbf{2}^{2+}$, $\mathbf{2}^{3+}$, $\mathbf{3}^{-}$, **3**, and $\mathbf{3}^{+}$ using the TD-DFT formalism[29] in acetonitrile using conductor-like polarizable continuum model.[30] *Chemissian 1.7*[31] was used to calculate the fractional contributions of various groups to each molecular orbital. All calculated structures were visualized with *ChemCraft*.[32]

Synthesis of $[Ru^{II}(L)(bpy)_2]ClO_4$ ($[\mathbf{1}]ClO_4$). A total of 100 mg (0.2 mmol) of $Ru(bpy)_2Cl_2·2H_2O$ and 83 mg (0.4 mmol) of $AgClO_4$ were taken in 30 mL of ethanol/water (2:1). The resulting mixture was refluxed under dinitrogen for 1 h. The precipitated AgCl was filtered off, and to the filtrate were added 37 mg (0.2 mmol) of HL and 21 mg of NEt_3 (freshly distilled over KOH; 0.2 mmol). The whole mixture was refluxed under a dinitrogen atmosphere for 6 h. The initial reddish-brown color of the solution gradually changed to dark-red violet. The reaction mixture was evaporated to dryness. The crude product was purified by using a neutral alumina column. The pure-red-violet complex $[\mathbf{1}]ClO_4$ was eluted by a solvent mixture of 5:1 dichloromethane/acetonitrile. Evaporation of the solvent under reduced pressure yielded pure complex $[\mathbf{1}]ClO_4$ in solid form. Yield: 110 mg (81%). Anal. Calcd for $C_{33}H_{23}N_4O_6ClRu$: C, 55.98; H, 3.27; N, 7.91. Found: C, 55.88; H, 3.19; N, 7.96. ESI MS (in CH_3CN): *m*/*z* 608.89 corresponding to $\mathbf{1}^{+}$ (calcd $\mathbf{1}^{+}$: *m*/*z* 609.08). ^1H NMR in $(CD_3)_2SO$ [δ/ppm]: 8.82 (d, 8.24, 2H), 8.70 (d, 8.25, 2H), 8.65 (d, 5.50, 2H), 8.16 (t, 8.02, 2H), 8.05 (d, 7.33, 2H), 7.91 (t, 8.25, 4H), 7.78 (d, 5.50, 2H), 7.65 (t, 6.415, 2H), 7.43 (t, 7.73, 1H), 7.28 (t, 6.64, 2H), 6.88 (d, 9.62, 2H).

Synthesis of $[Ru^{III}(L)_2(bpy)]ClO_4$ ($[\mathbf{2}]ClO_4$). A mixture of 100 mg (0.26 mmol) of $Ru(bpy)Cl_3·H_2O$ and 164 mg (0.78 mmol) of $AgClO_4$ was taken in 30 mL of EtOH and refluxed under dinitrogen for 1.5 h. The precipitated AgCl was removed by filtration, and to the filtrate were added 102 mg (0.52 mmol) of HL and 57 mg (0.52 mmol) of NEt_3 (freshly distilled over KOH). The mixture was heated under reflux for 8 h. The initial blue-violet solution was gradually changed to dark reddish-brown. The reaction mixture was evaporated to dryness and purified by using a neutral alumina column. The dark-reddish-brown complex $[\mathbf{2}]ClO_4$ was eluted by a mixture of 2:1 dichloromethane/acetonitrile. The solid complex $[\mathbf{2}]ClO_4$ was obtained via evaporation of the solvent under reduced pressure. Yield: 150 mg (77%). Anal. Calcd for $C_{36}H_{22}N_2O_6ClRu$: C, 57.83; H, 2.97; N, 3.75. Found: C, 57.83; H, 2.98; N, 3.78. ESI MS (in CH_3CN): *m*/*z* 647.86 corresponding to $\mathbf{2}^{+}$ (calcd $\mathbf{2}^{+}$: *m*/*z* 648.06). ^1H NMR in $CDCl_3$ [δ/ppm]: 22.09, 19.36, 17.95, 13.99, 12.04, 11.59, 5.0, 9.0, −0.98, −3.83, −5.52.

Synthesis of $[Ru^{III}(L)_3]$ (3). A mixture of 50 mg (0.19 mmol) of $RuCl_3·3H_2O$, 112 mg (0.57 mmol) of HL, and 63 mg (0.57 mmol) of NEt_3 (freshly distilled over KOH) was taken in 30 mL of ethanol and refluxed under dinitrogen for 12 h. The reaction mixture was evaporated to dryness under reduced pressure and purified by a silica gel (60−120 mesh) column. The reddish-brown complex **3** was eluted by a solvent mixture of 10:1 dichloromethane/acetonitrile. The pure solid complex **3** was obtained upon evaporation of the solvent under reduced pressure. Yield: 85 mg (65%). Anal. Calcd for $C_{39}H_{21}O_6Ru$: C, 68.12; H, 3.08. Found: C, 68.09; H, 3.11. ESI MS (in CH_3CN): *m*/*z* 687.19 corresponding to $\mathbf{3}^{+}$ (calcd $\mathbf{3}^{+}$: *m*/*z* 687.04). ^1H NMR in $CDCl_3$ [δ/ppm]: 12.96, 11.96, 4.03, −3.32.

Caution! *Perchlorate salts are explosive and should be handled with care.*

ASSOCIATED CONTENT

Supporting Information

X-ray crystallographic files in CIF format for $[\mathbf{1}]ClO_4$ and $[\mathbf{2}]ClO_4$, DFT data sets for $\mathbf{1}^n$, $\mathbf{2}^n$, and $\mathbf{3}^n$ (Tables S1−S23), mass spectra of $[\mathbf{1}]ClO_4$, $[\mathbf{2}]ClO_4$, and **3** (Figure S1), ^1H NMR spectra of $[\mathbf{1}]ClO_4$, $[\mathbf{2}]ClO_4$, and **3** (Figure S2), DFT-optimized structures of $\mathbf{1}^{+}$, $\mathbf{2}^{+}$, and **3** (Figure S3), and calculated spin-density plots, absorption spectra, and TD-DFT data of $L^{\bullet}$ and $L^{\bullet 2-}$ (Figures S4−S7 and Tables S24 and S25). This material is available free of charge via the Internet at http://pubs.acs.org.

AUTHOR INFORMATION

Corresponding Author

*E-mail: kaim@iac.uni-stuttgart.de (W.K.), lahiri@chem.iitb.ac.in (G.K.L.).

Notes

The authors declare no competing financial interest.

ACKNOWLEDGMENTS

Financial support received from the Department of Science and Technology and the Council of Scientific and Industrial Research, New Delhi (India) (fellowship to A.D.), and the DAAD, FCI, and DFG (Germany) is gratefully acknowledged. X-ray structural studies for $[\mathbf{1}]ClO_4$ and $[\mathbf{2}]ClO_4$ were carried out at the National Single Crystal Diffractometer Facility, Indian Institute of Technology, Bombay. Special acknowledgment is made to the Sophisticated Analytical Instrument Facility (SAIF), Indian Institute of Technology, Bombay, for providing the NMR facility.

REFERENCES

(1) (a) Fackler, J. P. Jr. *Prog. Inorg. Chem.* **1966**, *7*, 361. (b) Fortman, J. J. *Coord. Chem. Rev.* **1971**, *6*, 331. (c) Fay, R. C. *Coord. Chem. Rev.* **1996**, *154*, 99. (d) Rees, W. S. Jr. *Coord. Chem. Rev.* **2000**, *210*, 279. (e) Eaton, D. R. *J. Am. Chem. Soc.* **1965**, *87*, 3097. (f) Bullen, G. J.; Mason, R.; Pauling, P. *Nature* **1961**, *189*, 291.

(2) (a) Condorelli, G. G.; Malandrino, G.; Fragalà, I. L. *Coord. Chem. Rev.* **2007**, *251*, 1931. (b) Meng, Q.; Witte, R. J.; May, P. S.; Berry, M. T. *Chem. Mater.* **2009**, *21*, 5801. (c) Malandrino, G.; Perdicaro, L. M. S.; Condorelli, G.; Fragalà, I. L.; Rossib, P.; Dapportob, P. *Dalton Trans.* **2006**, 1101. (d) Andrieux, M.; Gasquères, C.; Legros, C.; Gallet, I.; Herbst-Ghysel, M.; Condat, M.; Kessler, V. G.; Seisenbaeva, G. A.; Heintz, O.; Poissonnet, S. *Appl. Surf. Sci.* **2007**, *253*, 9091.

(3) Khusniyarov, M. M.; Bill, E.; Weyhermüller, T.; Bothe, E.; Wieghardt, K. *Angew. Chem., Int. Ed.* **2011**, *50*, 1652.

(4) (a) Kumbhakar, D.; Sarkar, B.; Maji, S.; Mobin, S. M.; Fiedler, J.; Urbanos, F. A.; Jimenez-Aparicio, R.; Kaim, W.; Lahiri, G. K. *J. Am. Chem. Soc.* **2008**, *130*, 17575. (b) Das, A. K.; Sarkar, B.; Duboc, C.; Strobel, S.; Fiedler, J.; Záliš, S.; Lahiri, G. K.; Kaim, W. *Angew. Chem.* **2009**, *121*, 4306; *Angew. Chem., Int. Ed.* **2009**, *48*, 4242. (c) Das, A. K.; Sarkar, B.; Fiedler, J.; Záliš, S.; Hartenbach, I.; Strobel, S.; Lahiri, G. K.; Kaim, W. *J. Am. Chem. Soc.* **2009**, *131*, 8895. (d) Das, D.; Sarkar, B.; Kumbhakar, D.; Mondal, T. K.; Mobin, S. M.; Fiedler, J.; Urbanos, F. A.; Jiménez-Aparicio, R.; Kaim, W.; Lahiri, G. K. *Chem.—Eur. J.* **2011**, *17*, 11030.

(5) (a) Mandal, S. K.; Samanta, S.; Itkis, M. E.; Jensen, D. W.; Reed, R. W.; Oakley, R. T.; Tham, F. S.; Donnadieu, B.; Haddon, R. C. *J. Am. Chem. Soc.* **2006**, *128*, 1982. (b) Pal, S. K.; Tham, F. S.; Reed, R. W.; Oakley, R. T.; Haddon, R. C. *Polyhedron* **2005**, *24*, 2076. (c) Sen, T. K.; Mukherjee, A.; Modak, A.; Ghorai, P. K.; Kratzert, D.; Granitzka, M.; Stalke, D.; Mandal, S. K. *Chem.—Eur. J.* **2012**, *18*, 54.

(6) (a) Ghumaan, S.; Sarkar, B.; Maji, S.; Puranik, V. G.; Fiedler, J.; Urbanos, F. A.; Jimenez-Aparicio, R.; Kaim, W.; Lahiri, G. K. *Chem.—Eur. J.* **2008**, *14*, 10816. (b) Maji, S.; Sarkar, B.; Mobin, S. M.; Fiedler, J.; Urbanos, F. A.; Jimenez-Aparicio, R.; Kaim, W.; Lahiri, G. K. *Inorg. Chem.* **2008**, *47*, 5204.

(7) (a) Bennett, M. A.; Chung, G.; Hockless, D. C. R.; Neumann, H.; Willis, A. C. *J. Chem. Soc., Dalton Trans.* **1999**, 3451. (b) Bennett, M. A.; Byrnes, M. J.; Willis, A. C. *Dalton Trans.* **2007**, 1077.

(8) (a) Padhi, S. K.; Tanaka, K. *Inorg. Chem.* **2011**, *50*, 10718. (b) Boone, S. R.; Pierpont, C. G. *Polyhedron* **1990**, *9*, 2267. (c) Das, D.; Mondal, T. K.; Dutta Chowdhury, A.; Weisser, F.; Schweinfurth, D.; Sarkar, B.; Mobin, S. M.; Urbanos, F. A.; Jiménez-Aparicio, R.; Lahiri, G. K. *Dalton Trans.* **2011**, *40*, 8377.

(9) Matsuzawa, H.; Ohashi, Y.; Kaizu, Y.; Kobayashi, H. *Inorg. Chem.* **1988**, *27*, 2981.

(10) (a) Burgess, J.; Fawcett, J.; Russell, D. R.; Gilani, S. R. *Acta Crystallogr., Sect. C* **2000**, *C56*, 649. (b) Lebrun, P. C.; Lyon, W. D.; Kuska, H. A. *J. Crystallogr. Spectrosc. Res.* **1986**, *16*, 889.

(11) Braterman, P. S.; Song, J.-I.; Wimmer, F. M.; Wimmer, S.; Kaim, W.; Klein, A.; Peacock, R. D. *Inorg. Chem.* **1992**, *31*, 5084.

(12) Kaim, W.; Reinhardt, R.; Sieger, M. *Inorg. Chem.* **1994**, *33*, 4453.

(13) Kaim, W.; Ernst, S.; Kasack, V. *J. Am. Chem. Soc.* **1990**, *112*, 173.

(14) Weil, J. A.; Bolton, J. R.; Wertz, J. E. *Electron Paramagnetic Resonance*; Wiley: New York, 1994; p 532.

(15) (a) Reynolds, P. A.; Cable, J. W.; Sobolev, A. N.; Figgis, B. N. *J. Chem. Soc., Dalton Trans.* **1998**, 559. (b) Jarrett, H. S. *J. Chem. Phys.* **1957**, *27*, 1298.

(16) Kaim, W. *Coord. Chem. Rev.* **1987**, *76*, 187.

(17) Kaim, W. *Coord. Chem. Rev.* **2011**, *255*, 2503.

(18) (a) Ortiz de Montellano, P. T. *Chem. Rev.* **2010**, *110*, 932. (b) Phillippi, M. A.; Goff, H. M. *J. Am. Chem. Soc.* **1982**, *104*, 6026. (c) Kaim, W.; Schwederski, B. *Coord. Chem. Rev.* **2010**, *254*, 1580.

(19) Morita, Y.; Kawai, J.; Nishida, S.; Fukui, K.; Nakazawa, S.; Sato, K.; Shiomi, D.; Takui, T.; Nakasuji, K. *Polyhedron* **2003**, *22*, 2205.

(20) (a) Pal, S. K.; Itkis, M. E.; Tham, F. S.; Reed, R. W.; Oakley, R. T.; Haddon, R. C. *J. Am. Chem. Soc.* **2008**, *130*, 3942. (b) Svensson, C.; Abrahams, S. C.; Bernstein, J. L.; Haddon, R. C. *J. Am. Chem. Soc.* **1979**, *101*, 5759. (c) Rossetti, R.; Rayford, R.; Haddon, R. C.; Brus, L. E. *J. Am. Chem. Soc.* **1981**, *103*, 4303. (d) Rossetti, R.; Haddon, R. C.; Brus, L. E. *J. Am. Chem. Soc.* **1980**, *102*, 6913.

(21) Kaim, W. *Eur. J. Inorg. Chem.* **2012**, 343.

(22) Krause, R. A. *Inorg. Chim. Acta* **1977**, *22*, 209.

(23) Haddon, R. C.; Rayford, R.; Hirani, A. M. *J. Org. Chem.* **1981**, *46*, 4587.

(24) Krejcik, M.; Danek, M.; Hartl, F. *J. Electroanal. Chem.* **1991**, *317*, 179.

(25) Sheldrick, G. M. *SHELX-97, Program for Crystal Structure Solution and Refinement*; University of Göttingen: Göttingen, Germany, 1997.

(26) Lee, C.; Yang, W.; Parr, R. G. *Phys. Rev. B* **1988**, *37*, 785.

(27) (a) Dunning, T. H., Jr.; Hay, P. J. In *Modern Theoretical Chemistry*; Schaefer, H. F., III, Ed.; Plenum: New York, 1976; p 1. (b) Hay, P. J.; Wadt, W. R. *J. Chem. Phys.* **1985**, *82*, 299.

(28) Frisch, M. J.; Trucks, G. W.; Schlegel, H. B.; Scuseria, G. E.; Robb, M. A.; Cheeseman, J. R.; Montgomery, J. A., Jr.; Vreven, T.; Kudin, K. N.; Burant, J. C.; Millam, J. M.; Iyengar, S. S.; Tomasi, J.; Barone, V.; Mennucci, B.; Cossi, M.; Scalmani, G.; Rega, N.; Petersson, G. A.; Nakatsuji, H.; Hada, M.; Ehara, M.; Toyota, K.; Fukuda, R.; Hasegawa, J.; Ishida, M.; Nakajima, T.; Honda, Y.; Kitao, O.; Nakai, H.; Klene, M.; Li, X.; Knox, J. E.; Hratchian, H. P.; Cross, J. B.; Bakken, V.; Adamo, C.; Jaramillo, J.; Gomperts, R.; Stratmann, R. E.; Yazyev, O.; Austin, A. J.; Cammi, R.; Pomelli, C.; Ochterski, J. W.; Ayala, P. Y.; Morokuma, K.; Voth, G. A.; Salvador, P.; Dannenberg, J. J.; Zakrzewski, V. G. ; Dapprich, S.; Daniels, A. D.; Strain, M. C.; Farkas, O.; Malick, D. K.; Rabuck, A. D.; Raghavachari, K.; Foresman, J. B.; Ortiz, J. V.; Cui, Q.; Baboul, A. G.; Clifford, S.; Cioslowski, J.; Stefanov, B. B.; Liu, G.; Liashenko, A.; Piskorz, P.; Komaromi, I.; Martin, R. L.; Fox, D. J.; Keith, T.; Al-Laham, M. A.; Peng, C. Y.; Nanayakkara, A.; Challacombe, M.; Gill, P. M. W.; Johnson, B.; Chen, W.; Wong, M. W.; Gonzalez, C.; Pople, J. A. *Gaussian03*, revision C.02; Gaussian, Inc: Wallingford, CT, 2004.

(29) (a) Bauernschmitt, R.; Ahlrichs, R. *Chem. Phys. Lett.* **1996**, *256*, 454. (b) Stratmann, R. E.; Scuseria, G. E.; Frisch, M. J. *J. Chem. Phys.* **1998**, *109*, 8218. (c) Casida, M. E.; Jamorski, C.; Casida, K. C.; Salahub, D. R. *J. Chem. Phys.* **1998**, *108*, 4439.

(30) (a) Barone, V.; Cossi, M. *J. Phys. Chem. A* **1998**, *102*, 1995. (b) Cossi, M.; Barone, V. *J. Chem. Phys.* **2001**, *115*, 4708. (c) Cossi, M.; Rega, N.; Scalmani, G.; Barone, V. *J. Comput. Chem.* **2003**, *24*, 669.

(31) Leonid, S. *Chemissian 1.7*; 2005−2010. Available at http://www.chemissian.com.

(32) Zhurko, D. A. Zhurko, G. A. *ChemCraft 1.5*;Plimus: San Diego, CA. Available at http://www.chemcraftprog.com.